INEEL/CON-03-00550
PREPRINT

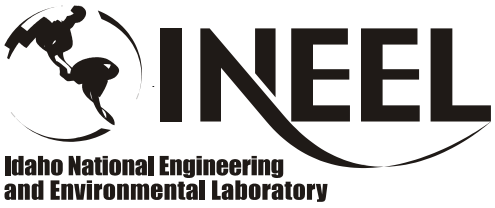

Modeling a Cold Crucible Induction Heated Melter

G. Hawkes

June 10, 2003 – June 11, 2003

2003 FIDAP/POLYFLOW User Group Meeting

Proceedings of 2003
FIDAP/POLYFLOW User Group Meeting
June 10-11, 2003, Evanston Illinois

MODELING A COLD CRUCIBLE INDUCTION HEATED MELTER

Grant Hawkes
Idaho National Engineering and Environmental Laboratory (INEEL)

ABSTRACT

FIDAP has been used to simulate melting of radioactive waste glass in a cold crucible induction heated melter. A model has been created that couples the magnetic vector potential (real and imaginary) to a transient startup of the melting process. This magnetic field is coupled to the mass, momentum, and energy equations that vary with time and position as the melt grows. The coupling occurs with the electrical conductivity of the glass as it rises above the melt temperature of the glass and heat is generated. Natural convection within the molten glass helps determine the shape of the melt as it progresses in time. An electromagnetic force is also implemented that is dependent on the electrical properties and frequency of the coil. This study shows the progression of the melt shape with time along with temperatures, power input, velocities, and magnetic vector potential. A power controller is implemented that controls the primary coil current and power.

INTRODUCTION

Cold Crucible Induction Melter (CCIM) design is based on inductive coupling of a water-cooled high-frequency electrical coil with the glass, causing eddy-currents that produce heat and mixing. Little data is available for engineering and economic evaluation of the CCIM technology, and no facilities are available in the US to support testing. FIDAP [1] is used to solve the electromagnetic field, coupled with the mass, momentum, and energy equations. This paper shows the startup transient of a proposed melter that is being built at the Idaho National Engineering and Environmental Laboratory (INEEL).

Figure 1 is a generic block diagram of a cold crucible induction heated melter system showing the eight major system components. While the ancillary systems are critical to the success of a vitrification process, the focus here is on research and development of the melter itself, including only the crucible, coil, and control system. The cooled crucible and induction coil are two key components of a CCIM system. In their simplest form they consist of a cylindrical single pass heat exchanger surrounded by a linear solenoid inductor. Figure 2 is a photograph of such a system currently being used at the V. G. Khlopin Radium Institute (KRI) in St. Petersburg, Russia for glass property studies [2]. This bench top system is approximately 9 cm in diameter and 40 cm tall. Note that both the crucible and the induction coil are cylindrical.

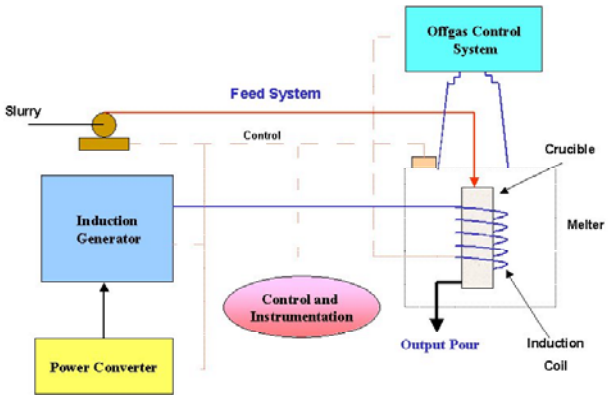

Figure 1. Schematic of CCIM system.

MODEL DESCRIPTION

The purpose of this model is to deterministically assess the transient startup of a melt configuration shown in Figure 3. Six turns of a 3/8-in copper coil tube are used as the primary coil current source. The crucible is not included in this model. A ring of a conductive material (1000 S/m) is used for the first 600 seconds of simulation. This is where the heat is generated until the glass reaches a temperature high enough to generate heat. After 600 seconds, the electrical conductivity of the material in the ring switches over to the electrical properties of glass for the remainder of the simulation. Running the simulation several times and adjusting this parameter found the time of 600 seconds. If a shorter time were used, then the melt would cool off and die and become the water temperature. In reality, a highly conductive material is placed in the melters for startup. The material gets consumed and mixed with the glass after convection starts.

Included in this model is natural convection of the glass as it is simulated in time. The melt grows and Navier-Stokes equations are solved for the convection within the melt that is driven by density differences. The heat transfer coefficient of 5.0 W/m^2-K on the outside of the hood area was chosen as a typical natural convection heat transfer coefficient.

A power controller is implemented in this model. The primary coil current is adjusted until the desired power is met. For this model, a power of 60 kW of induced heat is desired into the glass melt. We have purchased a 60 kW generator to be used in the laboratory experiment. A limit on the current is set at 70 Amps rms. The power is calculated with the FIDAP post processor and the current is adjusted at the next time interval by the ratio of the square root of the desired power versus actual power. Simply it is a proportional power controller.

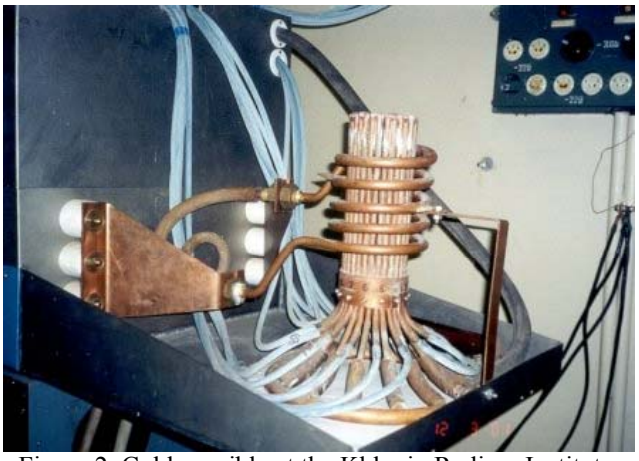

Figure 2. Cold-crucible at the Khlopin Radium Institute.

NOMENCLATURE

$\boldsymbol{A}$	vector potential, m-T
$\boldsymbol{I}$	overall electric current density = $\boldsymbol{J} + \boldsymbol{j}$
Q_e	RF-induced heat generation density, W/m^3
r,z	coordinate
T	temperature, K
t	time, s
$\boldsymbol{u}$	velocity vector, m/s
V	volume of each finite element

Greek letters

ϕ	modified vector potential with respect to azimuthal component, m^2-T
μ_e	permeability, H/m
σ_e	electrical conductivity, S/m
ω_e	angular frequency, rad/s

Subscript

c,s	cosine and sine component
r, θ, z	coordinate direction component

NUMERICAL FORMULATION

As shown in Figure 3, the main assumptions, which are used here, are as follows. (1) The system is axi-symmetric. (2) The induction coil is a six-turn coil with annular cross section. (3) An AC current is applied to the induction coil. (4) Natural convection within the melt is considered. Details of the numerical formulation are taken from Reference [3] and are as follows.

RF induced electromagnetic field

After expanding Maxwell's equations, the following equation for the magnetic vector potential is obtained:

$$\frac{\partial^2 A_\theta}{\partial r^2}+\frac{1}{r}\frac{\partial A_\theta}{\partial r}+\frac{\partial^2 A_\theta}{\partial z^2}-\frac{A_\theta}{r^2}=-\mu_e \mathbf{I} \qquad (1)$$

where A_θ is the azimuthal component of the magnetic vector potential **A**. By introducing a new variable ϕ named the modified vector potential where $\phi = rA_\theta$. After expanding Eq. 1, the following equation is obtained for ϕ.

$$\frac{\partial}{\partial r}\left(\frac{1}{r}\frac{\partial \phi}{\partial r}\right)+\frac{\partial}{\partial z}\left(\frac{1}{r}\frac{\partial \phi}{\partial z}\right)=-\mu_e I_\theta \qquad (2)$$

Note that Eq. (11) appears as a 2-D diffusion equation where the diffusivity term appears to be $\left(\frac{1}{r}\right)$. This is what is unique about this paper. FIDAP is used to solve this magnetic vector potential equation as a 2-D diffusion equation and use the magnetic vector potentials as a heat source for the axi-symmetric energy equation. Setting the diffusivity in equation 2 to be 1/r does this. It must be noted that these magnetic vector potentials are amplitudes and not rms values.

The modified vector potential is expressed as follows:

$$\phi = \phi_c \cos(\omega_e t) + \phi_s \sin(\omega_e t) \qquad (3)$$

By substituting Eq. (3) into Eq. (2) and using the relations from Reference 1, the following equations are obtained:

$$\frac{\partial^2 \phi_c}{\partial r^2} + \frac{\partial^2 \phi_c}{\partial z^2} - \frac{1}{r}\frac{\partial \phi_c}{\partial r} = \mu_e \sigma_e \omega_e \phi_s \qquad (4)$$

$$\frac{\partial^2 \phi_s}{\partial r^2} + \frac{\partial^2 \phi_s}{\partial z^2} - \frac{1}{r}\frac{\partial \phi_s}{\partial r} = -\mu_e \left(r J_\theta + \sigma_e \omega_e \phi_c \right) \qquad (5)$$

This is implemented in FIDAP by setting the source term in the FIDAP subroutine as follows:

Coil: 0 for Eq. 4
$\mu_e J_\theta$ for Eq. 5

Glass: $\dfrac{-\mu_e \sigma_e \omega_e \phi_s}{r}$ for Eq. 4

Air/space: 0 for Eq. 4 and 5

$\dfrac{\mu_e \sigma_e \omega_e \phi_c}{r}$ for Eq. 5

Heat generation rate is: $Q_e = \dfrac{\sigma_e \omega_e^2}{2r^2}\left(\phi_c^2 + \phi_s^2\right)$ (6)

Also from Reference [3], the electromagnetic force $_e$ that affects the melt motion is included.

Exact comparison with FIDAP for electromagnetic equations

When Eq. 2 is expanded, it becomes:

$$\frac{1}{r}\frac{\partial^2 \phi}{\partial r^2} - \frac{1}{r^2}\frac{\partial \phi}{\partial r} + \frac{1}{r}\frac{\partial^2 \phi}{\partial z^2} = -\mu_e I_\theta \qquad (7)$$

An arbitrary function of ϕ was chosen as:

$$\phi = r^5 + z^5 \qquad (8)$$

When solving for Eq. 8 in the form of Eq. 7 yields:

$$\frac{1}{r}\frac{\partial^2 \phi}{\partial r^2} - \frac{1}{r^2}\frac{\partial \phi}{\partial r} + \frac{1}{r}\frac{\partial^2 \phi}{\partial z^2} = 15r^2 + 20\frac{z^3}{r} \qquad (9)$$

with a computational domain of $0 \le r \le 1$, $0 \le z \le 1$ and with boundary conditions that satisfy Eq. 19 along the boundaries. Using these boundary conditions and solving the problem with FIDAP as a steady-state 2-D problem, and setting the species diffusivity = 1/r, the FIDAP results and the exact solution of Eq. 8 were compared along lines at z = 0.5 and at r = 0.5. The FIDAP results were within 1e-5 of the exact solution. This gives us the use of FIDAP to solve Eqs. 4 and 5 with the same technique of setting the diffusivity to 1/r and solving a 2-D diffusion problem.

Governing equations
The governing equations of transient laminar natural convection are solved.

Boundary conditions

(a) At the computational domain boundaries
$$\phi_c = 0, \quad \phi_s = 0 \qquad (10)$$
(b) At glass/air interface
$$Vz = 0, \; Vr = \text{free} \qquad (11)$$
(c) At the center (r=0)
$$\frac{\partial T}{\partial r} = 0, \; \phi_c = 0, \quad \phi_s = 0 \qquad (12)$$
(d) Gray body radiation from surface to surface in the enclosed air space at the top of the model. Heat flux boundary conditions as described in FIDAP theory manual.
(e) Convective heat transfer on outside of hood

Material properties

Table 1. Material properties for glass frit melt material. Only a portion of properties are shown, contact author..

μ_e = 1.257e-6 H/m, T_{ref} = 290 K, ρ_0 = 2801 kg/m^3

Temp (K)	σ_e (S/m)	μ (kg/m-s)	c_p (J/kg-K)	k (W/m-K)	β_T (1/K)
290	0.001	1.6e9	696	0.813	3.25e-5
973		5455	1710		6.43e-5
1073	0.001	376.5			
1173	3.333	61.59			8.16e-5
1273	6.63	16.66			
1373	12.45	6.20		1.0	9.16e-5
1473	19.41	2.86		2.0	
1973	45.80	0.31		18.36	1.08e-4
3000	100.0	0.31	1710	39.69	1.09e-4

Initial conductive region: all properties are same as glass, except σ_e = 1000 S/m for first 600 seconds.
Air properties: k = 0.1 W/m-K, ρ = 1.0 kg/m^3, c_p = 1005 J/kg-K

NUMERICAL PROCEDURE

The governing equations were solved with FIDAP. At time equal to zero and the temperature field initialized at 290 K, Eqs 4 and 5 were simultaneously solved over the domain for the real and imaginary portion of the modified magnetic vector potential. This was done in a separate problem of FIDAP and solved as a 2-D problem. An initial primary coil current of 59 Amps (rms) was guessed at time equal to zero. After convergence, the FIDAP post processor was used to calculate the power input into the melt region. The ϕ_c and ϕ_s were then used in Eq. 6 that is used as the heat source for axi-symmetric energy equation. The transient heat transfer and fluid flow calculation then proceeded for a period of five seconds and then stopped. The power controller was then implemented by introducing a new current source into the next time-step of the electromagnetic equations. The new primary coil current was controlled with a proportional controller as the square root of the desired power over the calculated power. The current was limited to not exceed 70 Amps. With this new current, the temperatures at the end of the five-second heat transfer calculation were used to calculate a new electromagnetic field. The electrical conductivity corresponding to these temperatures were used in Eqs. 4 and 5 and solved as a steady state problem. After convergence, the ϕ_c and ϕ_s were fed into the transient heat transfer as a heat source and the calculations proceeded from five seconds to 10 seconds. This process was repeated for until the time reached 3000 seconds. The time period for each calculation was 1.05 times larger than the time before. In short, the heat source remained constant during each transient heat transfer calculational period, and was then updated the next period as the melt grew and the electrical conductivity of the glass changed with time and position. The size and location of the initial conductive region was arrived at by several iterations that would allow the melt to continue to grow and not cool down and die. The results of these calculations will be shown in the Results section.

RESULTS AND DISCUSSION

Heat transport and melting due to induction heating for a glass frit in a CCIM have been performed for a transient startup for 3000 seconds. The numerical results are shown in Figures 4 through 20.

Figure 4 shows the finite element mesh, while Figure 5 shows a zoomed in view of the mesh used for the glass frit. Figure 6 shows the mesh for the coil, glass, and air. The initial conductive region is not plotted to show its size and location. 7700 four node quadrilateral elements were used.

Figures 7 and 8 show the imaginary and real modified magnetic vector potential at time=0. Notice that the high conductive region acts as a negative source as shown in Eq. 4. This region is shown as the blue area in Figure 8 and as a small island of blue in Figure 7.

Figures 9 through 14 show the velocity vectors for the melt as it progresses with time. The times for these figures are at 50, 100, 500, 1000, 2000, and 3000 seconds. Colors are associated with velocity magnitude. An isotherm of 1373 K is displayed in the figures. Figures 9 through 14 also show the temperature contours varying with time. All of the temperature contour lines are as shown in Figure 9.

The velocity vector reference magnitude for Figures 10 through 14 are noted in (m/s) as:

100 s, Vref = 0.1766e-2 1000 s, Vref = 0.5311e-2 3000 s, Vref = 0.3531e-1
500 s, Vref = 0.5204e-2 2000 s, Vref = 0.8593e-2

These figures show that the melt progresses upward and radially inward with time. The velocity greatly affects the shape of the melt as it transports the heat to the top and progresses the melt upwards. Two convective cells are formed for the majority of the transient. The flow goes downward near the outer wall, as this is the only place for the cooling to occur. This is also the region where the majority of the heat is generated since it is closest to the coil. This induces the flow to go upwards in the center and cool along the inner and outer walls.

Figures 15 and 16 show the heat generation rate in W/m^3 at 1000 and 2500 seconds respectively. Notice how the most heat is generated near the center of the coil in Figure 15 and also where the temperature is the highest and hence the higher electrical conductivity. Figure 16 shows a balance between these two facts as the higher temperature exists at the top, yet the most heat is generated near the center of the coil and as the magnetic vector potentials show in Figures 7 and 8 and taking into account the heat generation equation Eq. 6.

Figures 17 and 18 show the imaginary and real modified magnetic vector potential at 3000 seconds. Notice that the blue island area is not as pronounced and that the region has moved upward where the higher temperature and higher electrical conductivity is. The maximum value for the imaginary component in Figure 17 is lower than in the previous Figure 7. This is due to the current not being as high and hence not as much current source. The current is lower because the melt resistance has increased with a larger melt volume.

Temperature contours are displayed in Figure 19 of the entire heat transfer area at 2500 seconds. The top of the hood is receiving radiation heat transfer from the molten glass and has increased in temperature. The crucible wall stays at 290 K and receives a lot of radiation heat transfer since it is so close to the hottest portion of the melted surface. FIDAP calculates radiation view factors from each element surface to each other element surface and treats it as a heat flux.

Shown in Figure 20 are the calculated power and current history. The power is shown with the red squares and the current is shown with blue circles. The desired power level is 60 kW. With the current limited to 70 Amps, the power generated at the start is 44 kW. As the melt grows, the power increases because the melt resistance decreases with a larger size. This is true for a constant current. As the power increases above the 60 kW at 500 seconds, the current starts to decrease in order to keep the power at 60 kW. At 600 seconds, the initial conductive ring changes electrical conductivity from 1000 S/m to that of glass ~40 S/m. This sudden change is not realistic, and future models will incorporate more advanced techniques for diffusing this material through the melt with time. Since this drop in electrical conductivity does not generate as much heat, the current is driven back up to its limit of 70 Amps at a time of 650 seconds. As the melt grows and the melt resistance decreases, the current necessary to keep the power at 60 kW decreases and eventually reaches a value of 44 Amps at a time of 3000 seconds.

CONCLUSIONS

A transient startup of a CCIM has been simulated for a time of 3000 seconds. Heat transport with natural convection melting was tracked with time with the commercial CFD code FIDAP. Two electromagnetic equations for the real and imaginary magnetic vector potentials were solved with FIDAP and used as an induced heat source into the melt material. The melt grew until all of the glass frit was melted.

A power controller was implemented by controlling the primary coil current with a proportional controller. The current was limited to 70 Amps while the power was controlled to 60 kW of induced heat into the melt.

ACKNOWLEDGMENTS

This work was sponsored by the U.S. Department of Energy. The Idaho National Engineering and Environmental Laboratory is operated by Bechtel, Babcock and Wilcox Idaho, LLC under contract number DE-AC07-99ID13727.

REFERENCES

1. "FIDAP Theory Manual version 8.6.2", Fluent Inc., Lebanon, New Hampshire
2. Dmitry Lopukh, "Process Research and Development of Equipment for the Solidification of Radioactive Waste Simulators by Induction Cold Crucible Melting", January 2003, Leningrad Electrotechnical Institute, Russia.
3. Tetsuo Munakata, Ichiro Tanasawa, "Study on silicon melt convection during the RF-FZ crystal growth process II. numerical investigation", Journal of Crystal Growth, 206 (1999) 27-36.

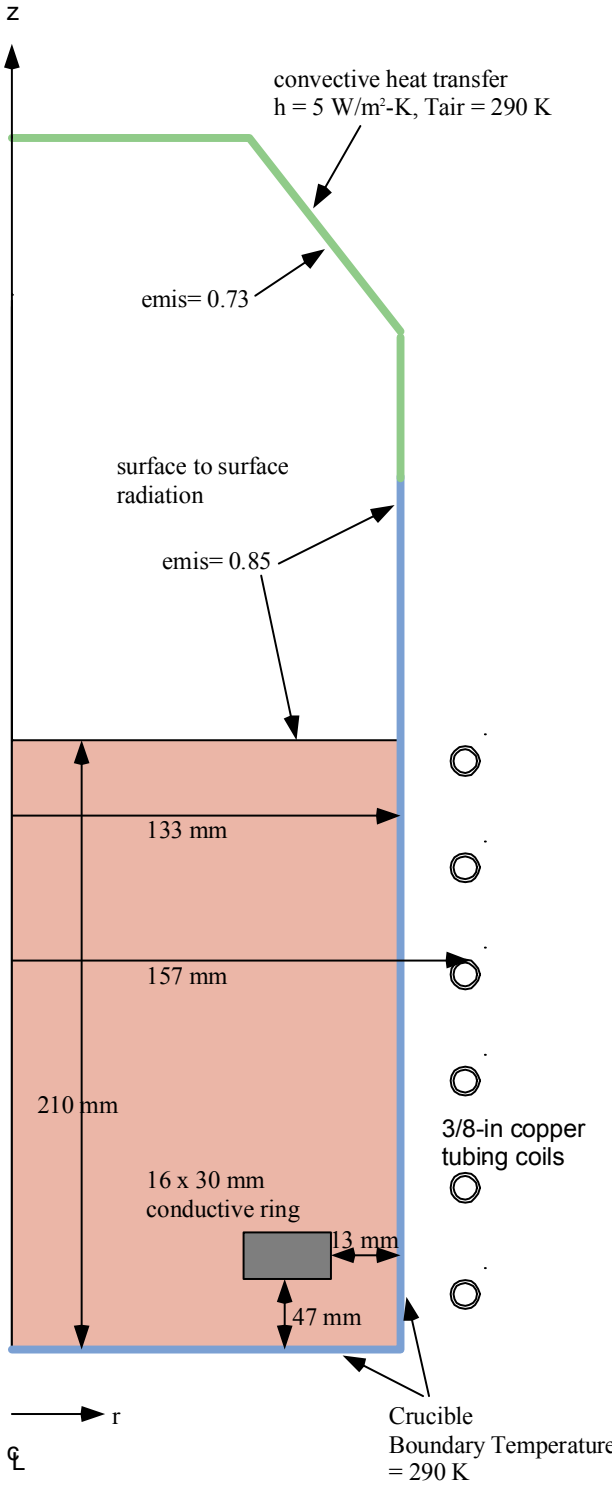

Figure 3. Model description.

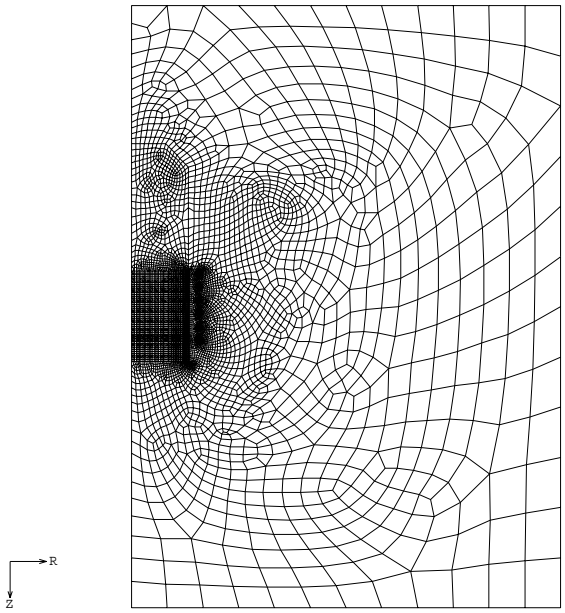

Figure 4. Finite element mesh.

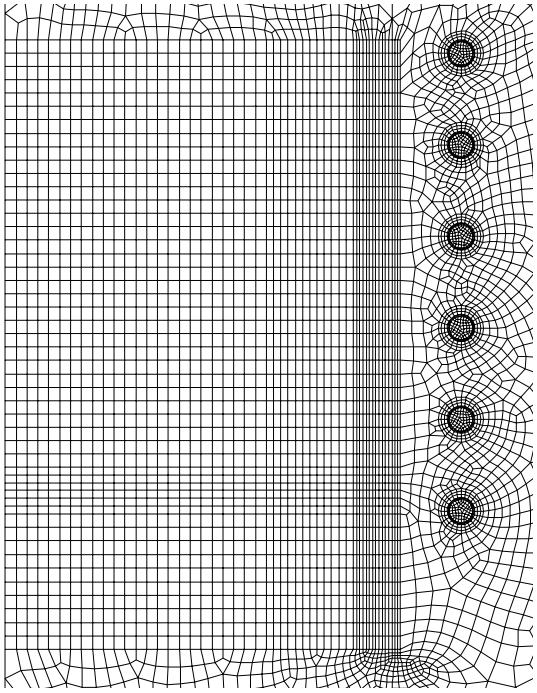

Figure 5. Zoomed in view of mesh near coils and melt area.

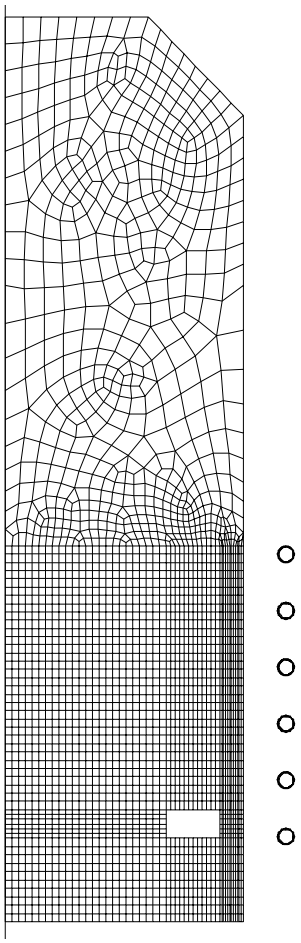

Figure 6. Mesh showing size of components.

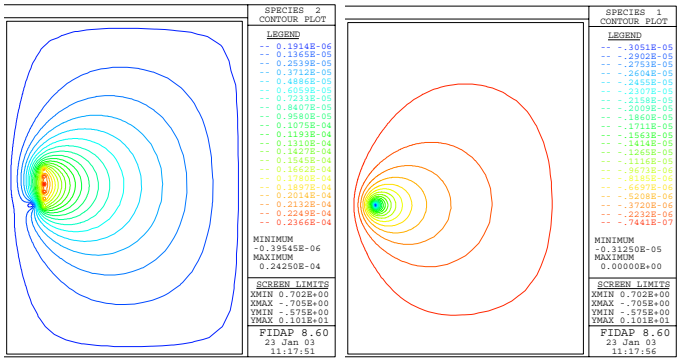

Figures 7 and 8. Imaginary and real magnetic vector potential contours plots, respectively.

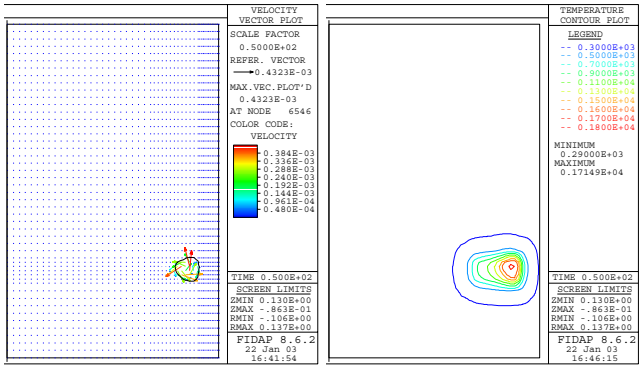

Figure 9. Velocity vectors and temperature contours at 50 seconds.

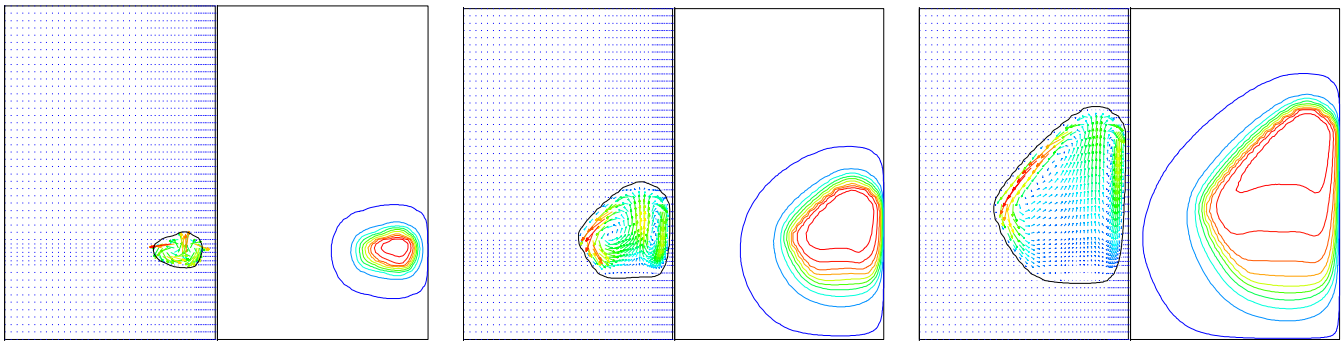

Figures 10, 11, and 12. Velocity vectors and temperature contours at 100, 500, and 1,000 seconds.

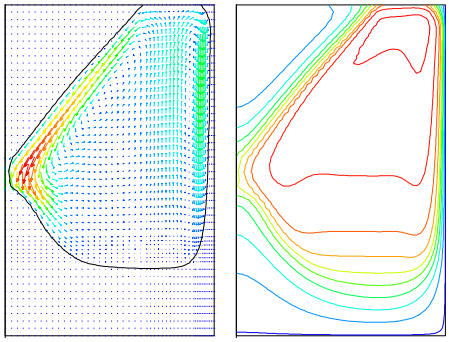

Figure 13. 2000 seconds

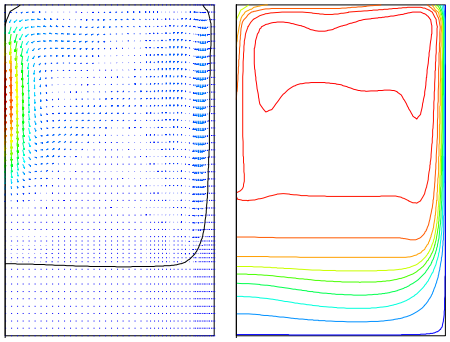

Figure 14. 3000 seconds

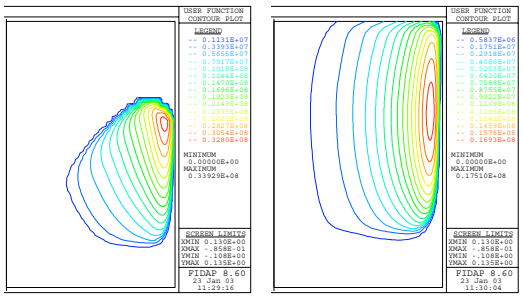

Figures 15 and 16. Heat generation rate at 1000 and 2500 seconds.

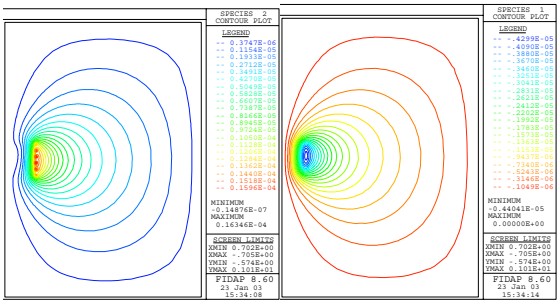

Figures 17 and 18. Imaginary and real magnetic vector potentials at 3000 seconds.

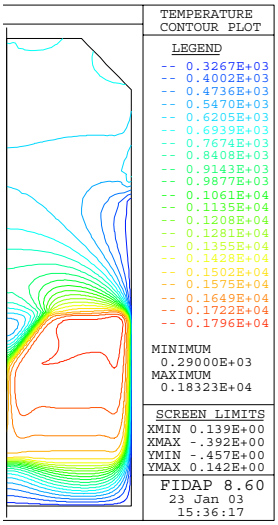

Figure 19. Temperature contours at 2500 seconds.

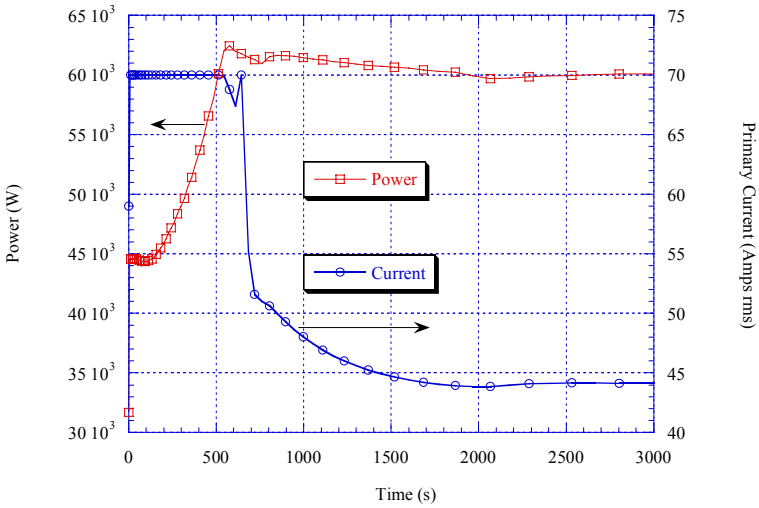

Figure 20. Induced power into the melt and primary coil current history.